Inelastic neutron scattering study of the lattice dynamics in the clathrate compound BaGe5

Christophe Candolfi, Umut Aydemir, Michael Marek Koza, Michael Baitinger, Yuri Grin, Franck Steglich

Inelastic neutron scattering study of the lattice dynamics in the clathrate compound $BaGe_5$

C. Candolfi,[1,2*] U. Aydemir,[1,3] M. M . Koza[4], M. Baitinger,[1] Yu. Grin[1], F. Steglich[1]

[1] *Max-Planck-Institut für Chemische Physik fester Stoffe, Nöthnitzer Str. 40, 01187 Dresden, Germany*

[2] *Institut Jean Lamour, UMR 7198 CNRS-Université de Lorraine, Parc de Saurupt, CS 50840 F-54011 Nancy Cedex, France*

[3] *Department of Applied Physics and Materials Science, California Institute of Technology, 1200 E California Blvd, Pasadena, CA 91125, United States*

[4] *Institut Laue Langevin, 6 rue Jules Horowitz, B.P. 156, 38042 Grenoble, Cedex 9, France*

[*] Corresponding author: christophe.candolfi@univ-lorraine.fr

Abstract

We report inelastic neutron scattering (INS) measurements on the polycrystalline *oP*60-type clathrate $BaGe_5$, whose crystal structure is related to the type-I clathrate $Ba_8Ge_{43}\square_3$ and to the *cP*124-clathrate Ba_6Ge_{25}. Our results show that $BaGe_5$ exhibits a similar phonon density of states (PDOS) in the energy range 0 – 40 meV with respect to $Ba_8Ge_{43}\square_3$. The low-energy region of the PDOS spectrum (0 – 10 meV) consists of two peaks at 4.1 and 6.2 meV likely related to Ba-weighted modes. Compared to $Ba_8Ge_{43}\square_3$, the low-energy region of the phonon spectrum of $BaGe_5$ shows a more complex structure, likely reflecting the presence of three distinct crystallographic sites for Ba. The specific heat data of $BaGe_5$, reexamined in light of

the INS results, indicate that the Ba-weighted modes dominate the low-temperature behavior of C_p.

I. Introduction

Cage-like structures represent an interesting playground to better understand the interplay between disorder, anharmonicity and thermal motion of encaged atoms under temperature and pressure variations. These features are at the core of the phonon-scattering events, which control the ability of the structure to conduct heat. A deeper understanding of the thermal transport of open-framework structures is therefore intimately related to their vibrational properties.[1]

Clathrate compounds represent a class of cage-like materials in which, low-energy vibrational modes due to the thermal motion of the encaged cations and the rotational degrees of freedom of gas molecules in clathrate hydrates are two prominent examples of microscopic mechanisms governing the thermal transport of these structures.[2-11] The coherent nature of the thermal motion of the filler atoms and the framework has strong influence on the thermal transport, which mimics that of amorphous solids. The combination with off-center position of the cations in the cages also results in glass-like thermal conductivity in some type-I clathrates $Sr_8Ga_{16}Ge_{30}$ and $Eu_8Ga_{16}Ge_{30}$.[12-15]

The variety of framework structures within the family of clathrates was recently enlarged with the discovery of a new structure type $BaGe_5$.[16,17] This compound crystallizes in the orthorhombic space group *Pmna*. The structure is characterized by Ge layers perpendicular to the [010] direction and interconnected by three-bonded Ge species (Figures 1a and 1b). The 2D infinite layers consist of Ge_{20} dodecahedra interconnected by pentagons and hexagons of Ge atoms. The crystal structure of $BaGe_5$ is closely related to those of two others cage-like

compounds in the Ba – Ge system $Ba_8Ge_{43}\square_3$ and Ba_6Ge_{25}: the arrangement of pentagons and hexagons is similar to the polyhedral cages in $Ba_8Ge_{43}\square_3$ while the presence of infinite channels is reminiscent to those in Ba_6Ge_{25}.[18-21] $BaGe_5$ is synthesized via a solid-solid reaction involving first the thermal decomposition of the phase $Ba_8Ge_{43}\square_3$ between 573 and 793 K into $BaGe_5$ and α-Ge, and then the formation of $BaGe_5$ by peritectoid reaction between Ba_6Ge_{25} and α-Ge.[16]

Detailed investigation of the transport, thermodynamic and magnetic properties of $BaGe_5$ for different annealing temperatures and times revealed that both parameters control the microstructure thereby likely influencing the transport properties.[17] The semiconducting $BaGe_5$ is an electron-precise Zintl phase with the charge balance $Ba^{2+}[(3b)Ge^-]_2[(4b)Ge^0]_3$ when considering the presence of three-bonded and four-bonded Ge atoms. One of the main differences between $BaGe_5$ and the related clathrate $Ba_8Ge_{43}\square_3$ is the presence of three distinct Ba sites (Figure 2) in the former while only two crystallographic sites host Ba in the latter. Specific heat measurements have shown that the additional contribution related to the thermal motion of the entrapped atoms is still present in $BaGe_5$.[17] These modes, that dominate the low-temperature C_p data, suggest a more complex phonon spectrum at low energy than in $Ba_8Ge_{43}\square_3$.

In the present work, we extend our experimental investigation of $BaGe_5$ by focusing on the lattice dynamics with the aim of unveiling similarities or differences with $Ba_8Ge_{43}\square_3$. For this purpose, we mapped out the powder-averaged dynamic structure factor $S(Q,E)$ at 300 and 100 K using inelastic neutron scattering experiments (INS). The generalized phonon density of states $G(E)$, derived from the $S(Q,E)$ function, is presented and discussed in light of the INS data obtained on $Ba_8Ge_{43}\square_3$ by Koza *et al.*[22] The low-temperature specific heat data, reported in Ref. 17, are reexamined here to explore the role played by the Ba-weighted phonon modes.

II. Experimental details

A. Synthesis, structural and chemical characterizations of $BaGe_5$

A polycrystalline sample of $BaGe_5$ was synthesized from the decomposition of the parent compound $Ba_8Ge_{43}\square_3$ obtained by a steel-quenching of the melt.[23] Bulk pieces of $Ba_8Ge_{43}\square_3$ were placed in glassy carbon crucibles sealed in quartz ampoules under Ar atmosphere. The ampoules were annealed at 673 K for four days and finally quenched in water. $BaGe_5$ can be obtained by varying the annealing temperature between 623 and 793 K.[16,17] While subtle differences in the crystal structure could not be strictly ruled out, variations in the phonon density of states with annealing conditions seem unlikely. In this study, we therefore restrict ourselves to a material annealed at one temperature.

Powder X-ray diffraction (PXRD) measurements indicated that $BaGe_5$ was successfully formed together with a small amount of elemental Ge (≈5 mass%) in agreement with the difference between the starting and final composition. The diffraction pattern obtained on IN6 is consistent with these observations (Figure 3). Full-profile refinement against room-temperature synchrotron X-ray data was carried out using the program package WinCSD.[24] While the Ba1 atoms centered in the dodecahedral cages were refined isotropically, the thermal displacement parameters of the Ba2 and Ba3 atoms were further refined anisotropically. The crystallographic parameters of $BaGe_5$ are listed in Table I. The comparison of these parameters with those reported in our prior structure investigation (Ref. 16) reveals no relevant differences in atomic positions and occupations. All the lattice parameters and atomic coordinates are equal within three estimated standard deviations. The obtained structure model is used hereafter for interpretation of the results of INS experiments as well as of specific heat measurements.

Specific heat measurements were performed from 2 to 300 K on a bulk piece (~ 20 mg)

under zero magnetic field using the dedicated option of a physical property measurements system (PPMS, Quantum Design).

B. Inelastic neutron scattering

INS experiments were performed at 300 and 100 K using the cold-neutron time-of-flight spectrometer IN6@ILL, located at the European neutron source Institut Laue Langevin (ILL) in Grenoble (France). The data were collected on a powder specimen (m ~ 15 g) with an incident neutron wavelength of 4.14 Å and with the time-focusing mode to ensure the best energy resolution at 7 meV. This setup allows a sampling of the entire dynamics of $BaGe_5$ on the anti-Stokes line (neutron energy gain). All measurements were performed in transmission geometry using flat aluminum sample holders. The sample was measured at 300 and 100 K for 8 and 12 h, respectively, to reach a good signal-to-noise ratio in the measured intensities. Measurement of the empty aluminum sample holder has been also performed at both temperatures.

The recorded response was corrected for empty sample holder scattering and normalized to pure-incoherent vanadium standard to account for detector efficiency. The data were processed to obtain the dynamic structure factor $S(Q,\omega)$ that was converted into the generalized phonon density of states $G(\omega)$. The incoherent approximation was utilized following conventional mathematical relations to determine $G(\omega)$.[25] The positions of the maxima in the PDOS spectrum were determined by fitting the data to a set of Gaussian functions.

III. Results and discussion

A. Generalized phonon density of states $G(\omega)$

Figure 4 shows the experimental $S(Q,\omega)$ plot in the whole energy range covered. Since the Q-dependence of the phonon signal reflects the features of the phonon structure factor, strongly dispersive acoustic bands originating from Bragg peaks are observable. Such dispersive branch dominates the low-energy region and extends up to ~ -3 meV. Above this energy, the inelastic signal is composed of several van Hove singularities visualized as intensity maxima.

The generalized density of states $G(\omega)$ of $BaGe_5$ obtained at 100 and 300 K are shown in Figure 5a as a function of the energy. The phonon spectrum of $BaGe_5$ features three pronounced peaks at about $\hbar\omega$ = 11.5, 30 and 35 meV dominating the overall profile up to the cutoff energy of ~ 40 meV in addition to several peaks and shoulders.[22] Although the profiles of $BaGe_5$ and $Ba_8Ge_{43}\square_3$ appear similar, these peaks are shifted towards higher energies in $BaGe_5$ with respect to $Ba_8Ge_{43}\square_3$ (see Table II).

To stress the low-energy features of the spectrum, a Debye plot $G(\omega)/(\hbar\omega)^2$ vs. $\hbar\omega$ is presented in Figure 5b. The strong rising intensity towards low energy stems from the elastic contribution of the Bragg peak seen in the $S(Q,\omega)$ maps. Because of this additional contribution, the $G(\omega)/(\hbar\omega)^2$ data depart from a Debye characteristic for which $G(\omega)/(\hbar\omega)^2\big|_{\hbar\omega\to 0} = cst$. The inelastic signal shows several peaks and shoulders at 4.1, 6.8 and 9.7 meV. In particular, the peak centered at 6.8 meV is broad and possibly composed of two separated peaks at 6.2 and 7.6 meV. We stress here that, due to the different scattering powers of Ba and Ge (0.0246 and 0.118 barns/amu, respectively), which results in an intensity

modification of $G(\omega)$ with respect to the vibrational density of states $Z(\omega)$ calculated from *ab initio* calculations, the INS measurements are more sensitive to Ge atoms. Nevertheless, following the assignment of the modes in $Ba_8Ge_{43}\square_3$, we may conclude that these low-energy peaks, which are located at lower energies than their counterparts in $Ba_8Ge_{43}\square_3$ (see Table II), are related to collective modes involving Ba atoms.[22] Hence, the more complex structure of the low-energy region compared to the type-I clathrate likely reflects the more complex crystal structure of $BaGe_5$ with three distinct crystallographic sites for Ba and additional local differences in the Ba environment caused by the disorder at the Ge4 and Ge5 positions (see Table I).

Upon cooling, the entire spectrum shifts towards higher energies due to the decrease in the unit cell volume (Figure 5b). This shift can be usually accounted for within the quasiharmonic model, which allows predicting the temperature dependence of the phonon frequencies by utilizing the linear thermal expansion coefficient and the Grüneisen parameter that measures the response of the phonon modes upon a volume change. Within this model, the quasiharmonic phonon energies $E_i^{qh}(T)$ may be expressed as[26,27]

$$E_i^{qh}(T) = E_i^{300K}\left(1-\bar{\gamma}\frac{V(T)-V_{300K}}{V_{300K}}\right) \quad (1)$$

where E_i^{300K} is the value of the *i*th phonon energy measured at 300 K, $\bar{\gamma}$ is the thermodynamic Grüneisen parameter that stands for the average value of the Grüneisen parameter of each phonon mode $\gamma_i = \left(-\frac{1}{\hbar}\frac{\partial \ln E_i}{\partial \ln V}\right)_T$ and $V(T)$ is the volume of the unit cell at temperature T. The Grüneisen parameter $\bar{\gamma}$, assumed to be temperature-independent herein, was calculated at 300

K using the relation $\bar{\gamma} = 3\alpha_T BV / C_v \approx 3\alpha_T BV / C_p$ where α_T is the linear thermal expansion coefficient, B is the isothermal bulk modulus and C_v and C_p are the specific heat at constant volume and pressure, respectively. Due to the similarities of the crystal structures and the overall close match of $G(\omega)$ of $BaGe_5$ and $Ba_8Ge_{43}\square_3$, α_T and B determined for the latter (α_T = 12.65×10^{-6} K^{-1} and B = 52.8 GPa) were used in the present case yielding $\bar{\gamma} \approx$ 1.2.[28] As a first approximation, an isotropic α_T value has been assumed despite the anisotropic unit cell of $BaGe_5$. The quasiharmonic prediction of the temperature dependence of the main peaks is shown in Figure 6. In spite of the simplifications used in the present case, the slight shift in the energies upon cooling is well accounted for by this model to within experimental uncertainty. This result contrasts with the softening expected in the case of strongly anharmonic modes as observed in other materials such as pyrochlores, $A V_2Al_{20}$ (A = Sc, La, Ce) or tetrahedrites and suggests the absence of significant anharmonicity in $BaGe_5$ as similarly observed in $Ba_8Ge_{43}\square_3$.[22,29-31] Further, this indicates that the local disorder in the Ge framework present in both structures does not give rise to anharmonicity beyond the quasi-harmonic approximation.

B. Specific heat

Figure 7 depicts the temperature dependence of the specific heat C_p between 2 and 100 K plotted as C_p / T^3 vs. T. In type-I clathrates, deviation from a conventional Debye behavior can be observed and manifests itself as a maximum typically centered near 15 K.[15,18,32-34] This deviation reflects the lowest energy features related to the anisotropic thermal motion of the Ba atoms inside the tetrakaidecahedra (see Table I). Our previous study has shown that this maximum is still present when $Ba_8Ge_{43}\square_3$ transforms into $BaGe_5$.[17] However, in $BaGe_5$, the presence of one additional Ba site makes the analysis more complicated since several models

may equivalently describe the C_p data. Keeping in mind that the specific heat is not a probe sensitive enough to discern the fine details of the low-energy PDOS and that the use of a restricted set of temperature-independent parameters cannot describe accurately the C_p data in an extended temperature range, we tried, as a first approximation and in light of the INS data collected, to model the low-temperature $C_p(T)$ region in a manner similar to type-I clathrates. In this model, the lattice specific heat C_L is decomposed into one Debye contribution and two Einstein terms

$$C_L(T) = 9N_D R\left(\frac{T}{\theta_D}\right)^3 \int_0^{\theta_D/T} \frac{x^4 e^x}{(e^x-1)^2} dx + p_1 N_{E1} R\left(\frac{\theta_{E1}}{T}\right)^2 \frac{e^{\theta_{E1}/T}}{(e^{\theta_{E1}/T}-1)^2} + p_2 N_{E2} R\left(\frac{\theta_{E2}}{T}\right)^2 \frac{e^{\theta_{E2}/T}}{(e^{\theta_{E2}/T}-1)^2} \quad (2)$$

where N_D is the number of Debye oscillators, θ_D is the Debye temperature, N_{E1} and N_{E2} are the number of Einstein oscillators, θ_{E1} and θ_{E2} are the Einstein temperatures and p_1 and p_2 their spectral weights that equal to 1, 2 or 3 for one-, two- or three-dimensional vibrations, respectively. We used two Einstein terms to describe the peaks located at 4.1 and 6.2 meV in the PDOS, which correspond to Einstein temperatures of θ_{E1} = 48 and θ_{E2} = 72 K, respectively. These two temperatures were kept constant during the fitting procedure. The number of Debye oscillators was constrained to N_D = 5.6 (5 Ge atoms, 0.2 Ba1 atoms, one third of Ba2 atoms and two-third of Ba3 atoms per chemical formula) while $p_1 N_{E1}$ and $p_2 N_{E2}$ were free parameters. The best fit to the data yields θ_D = 240 K, $p_1 N_{E1}$ = 0.47 and $p_2 N_{E2}$ = 1.05 and, as shown in Figure 7, this model captures reasonably well the low-temperature peak observed. We note that the quality of the fit was significantly improved with two Einstein temperatures while the use of only one characteristic temperature did not produce a satisfying description of the data in this temperature range. X-ray synchrotron data revealed that the

thermal ellipsoid of the Ba2 atoms is "flattened" along the [100] direction ($U_{11} < U_{22} \approx U_{33}$), while the Ba3 atoms display a more pronounced anisotropic behavior ($U_{33} < U_{11} < U_{22}$, see Table I). If we further assume that p_1 and p_2 reflect the Ba3 and Ba2 atoms, respectively, these parameters should then take the respective values of 1 and 2. Given that N_{E1} and N_{E2} equal to one third and two third, respectively, we would thus expect $p_1 N_{E1}$ and $p_2 N_{E2}$ to be equal to 0.133 and 1.33, respectively. The values derived from Eq.(2) roughly correspond to these values suggesting that the peaks in the PDOS spectrum located at 4.1 and 6.2 meV may be ascribed to the Ba3 and Ba2 atoms, respectively. This is consistent with the fact that higher thermal displacement parameters are related to reduced restoring forces resulting in lower Einstein energies and hence, in lower energy modes in the PDOS spectrum.

IV. Conclusion

In the present paper, we reported results from time-of-flight neutron spectroscopy and specific heat measurements on the clathrate compound $BaGe_5$. Because the crystal structure of $BaGe_5$ derives from that of the type-I clathrate $Ba_8Ge_{43}\square_3$ with respect to the Ba environment and Ge connectivity, the overall PDOS spectrum displays a similar structure. Of relevance is the fact that the low-energy phonon spectrum features a more complex structure *i.e.* in the energy range where the Ba-weighted eigenmodes are expected to dominate. The collapse of the tetrakaidecahedra present in $Ba_8Ge_{43}\square_3$ leads to three distinct sites for Ba in $BaGe_5$ likely explaining these differences. The inelastic response upon cooling revealed a shift in the phonon energies that can be well understood within the quasiharmonic model. The low-temperature specific heat of $BaGe_5$ is dominated by the dynamics of the Ba2 and Ba3 atoms that can be well modeled by additional Einstein-like modes.

Acknowledgement

The authors thank Petra Scheppan, Renate Hempel-Weber and members of the Kompetenzgruppe Struktur for providing experimental support. C.C. acknowledges the financial support of the CNRS-MPG program. M.B. and Yu.G. gratefully acknowledge financial support by the Deutsche Forschungsgemeinschaft (SPP 1415, “Kristalline Nichtgleichgewichtsphasen (KNG) - Präparation, Charakterisierung und *in situ*-Untersuchung der Bildungsmechanismen”).

Tables

Table I. Atomic coordinates, displacement parameters (in Å^2) and site occupancies for $BaGe_5$ obtained at 673 K (Space group *Pmna* (no. 52); a = 10.7265(8) Å, b = 9.2839(5) Å, c = 14.791(1) Å; Z = 10).

Atom	**Site**	***x***	***y***	***z***	U_{eq} / U_{iso}	***Occ.***
Ba1	2*a*	0	0	0	0.013(1)	1.0
Ba2	*4g*	1/4	0.4236(3)	1/4	0.022(1)	1.0
Ba3	4*h*	0	0.2053(3)	0.6324(2)	0.036(2)	1.0
Ge1	4*h*	0	0.3647(5)	0.1105(3)	0.007(1)	1.0
Ge2	4*h*	0	0.2152(5)	0.3815(3)	0.005(1)	1.0
Ge3	4*h*	0	0.1454(5)	0.2141(3)	0.008(2)	1.0
Ge4	4*h*	0	0.4684(9)	0.4077(5)	0.010(3)	0.5*
Ge5	8*i*	0.3373(5)	0.5068(9)	0.0312(3)	0.005(2)	0.5*
Ge6	8*i*	0.3050(3)	0.0934(3)	0.0607(2)	0.0073(8)	1.0
Ge7	8*i*	0.1198(3)	0.7223(3)	0.1543(2)	0.0089(8)	1.0
Ge8	8*i*	0.1809(3)	0.3088(3)	0.0051(2)	0.0073(8)	1.0
Ge9	8*i*	0.3184(3)	0.0207(3)	0.6852(2)	0.0062(8)	1.0
Atom	U_{11}	U_{22}	U_{33}	U_{12}	U_{13}	U_{23}
Ba2	0.013(2)	0.026(2)	0.027(3)	0	-0.005(2)	0
Ba3	0.033(2)	0.054(3)	0.019(2)	0	0	-0.000(2)

U_{eq} is defined as one third of the trace of the orthogonalized U_{ij} tensor, which is $\exp(-2\pi^2 [h^2 a^{*2} U_{11} + \ldots + 2hka^*b^*U_{12}])$.

* Free refinement of the occupancies of Ge4 and Ge5 led to the values 0.510(5) and 0.500(3), respectively, which were fixed to 0.5 at the final stage of the refinement.

Table II. Comparison of the position of the van Hove singularities (in meV) inferred from INS data for $BaGe_5$ and $Ba_8Ge_{43}\square_3$ (Ref. 22).

$BaGe_5$	$Ba_8Ge_{43}\square_3$
4.1	4.8
6.2	/
7.6	8
9.7	/
11.3	9.5
14.3	13
22.5	18
25.5	23
30.1	28
35.1	32

References

[1] B. Fultz, *Prog. Mater. Sci.* **55**, 247 (2010).

[2] J. S. Tse, D. D. Klug, J. Y. Zhao, W. Sturhahn, E. E. Alp, J. Baumert, C. Gutt, M. R. Johnson and W. Press, *Nat. Mater.* **4**, 917 (2005).

[3] J. S. Tse and M. A. White, *J. Phys. Chem.* **92**, 5006 (1988).

[4] M. Christensen, A. B. Abrahamsen, N. B. Christensen, F. Juranyi, N. H. Andersen, K. Lefmann, J. Andreasson, C. R. H. Bahl, B. B. Iversen, *Nat. Mater.* **7**, 811 (2008).

[5] J. L. Cohn, G. S. Nolas, V. Fessatidis, T. H. Metcalf and G. A. Slack, *Phys. Rev. Lett.* **82**, 779 (1999).

[6] B. Chazallon, H. Itoh, M. M. Koza, W. F. Kuhs and H. Schober, *Phys. Chem. Chem. Phys.* **4**, 4809 (2002).

[7] M. M. Koza and H. Schober in *Neutron Applications in Earth, Energy and Environmental Sciences* (Springer), Chap. 12.

[8] S. Pailhès, H. Euchner, V. M. Giordano, R. Debord, A. Assy, S. Gomès, A. Bosak, D. Machon, S. Paschen and M. de Boissieu, *Phys. Rev. Lett.* **113**, 025506 (2014).

[9] H. Euchner, S. Pailhès, L. T. K. Nguyen, W. Assmus, F. Ritter, A. Haghighirad, Yu. Grin, S. Paschen and M. de Boissieu, *Phys. Rev. B* **86**, 224303 (2012).

[10] S. Christensen, L. Bjerg, A. Kaltzoglou, F. Juranyi, T. Fässler, T. Unruh and M. Christensen, *J. Appl. Phys.* **113**, 084902 (2013).

[11] T. Tadano, Y. Gohda and S. Tsuneyuki, *Phys. Rev. Lett.* **114**, 095501 (2015).

[12] B. C. Sales, B. C. Chakoumakos, R. Jin, J. R. Thompson and D. Mandrus, *Phys. Rev. B* **63**, 245113 (2001).

[13] R. Baumbach, F. Bridges, L. Downward, D. Cao, P. Chesler and B. C. Sales, *Phys. Rev. B* **71**, 024202 (2005).

[14] F. Bridges and L. Downward, *Phys. Rev. B* **70**, 140201 (2004).

[15] K. Suekuni, M. A. Avila, K. Umeo and T. Takabatake, *Phys. Rev. B* **75**, 195210 (2007).

[16] U. Aydemir, L. Akselrud, W. Carrillo-Cabrera, C. Candolfi, N. Oeschler, M. Baitinger, F. Steglich and Yu. Grin, *J. Am. Chem. Soc.* **132**, 10984 (2010).

[17] C. Candolfi, U. Aydemir, A. Ormeci, W. Carrillo-Cabrera, U. Burkhardt, M. Baitinger, N. Oeschler, F. Steglich and Yu. Grin, *J. Appl. Phys.* **110**, 043715 (2011).

[18] U. Aydemir, C. Candolfi, H. Borrmann, M. Baitinger, A. Ormeci, W. Carrillo-Cabrera, C. Chubilleau, B. Lenoir, A. Dauscher, N. Oeschler, F. Steglich and Yu. Grin, *Dalton Trans.* **39**, 1078 (2010).

[19] N. L. Okamoto, M. W. Oh, T. Nishii, K. Tanaka and H. Inui, *J. Appl. Phys.* **99**, 033513 (2006).

[20] H. G. von Schnering, A. Zürn, J.-H. Chang, M. Baitinger and Yu. Grin, *Z. Anorg, Allg. Chem.* **633**, 1147 (2007).

[21] W. Carrillo-Cabrera, R. Cardoso Gil, S. Paschen and Yu. Grin, *Z. Kristallogr. NCS* **218**, 397 (2003).

[22] M. M. Koza, M. R. Johnson, H. Mutka, M. Rotter, N. Nasir, A. Grytsiv and P. Rogl, *Phys. Rev. B* **82**, 214301 (2010).

[23] M. Baitinger, B. Böhme, A. Ormeci and Yu. Grin in *The Physics and Chemistry of Inorganic Clathrates*, Chap. 2, Ed. G. S. Nolas, Springer, 2014, p. 35 – 64.

[24] L. G. Akselrud, Yu. Grin, *J. Appl. Cryst.* **47**, 803 (2014).

[25] G. L. Squires in *Introduction to Thermal Neutron Scattering* (Dover, New York, 1996).

[26] O. L. Anderson, *Geophys. J. Int.* **143,** 279 (2000).

[27] L. Mauger, M. S. Lucas, J. A. Muñoz, S. J. Tracy, M. Kresch, Y. Xiao, P. Chow and B. Fultz, *Phys. Rev. B* **90**, 064303 (2014).

[28] M. Falmbigl, S. Puchegger and P. Rogl in *The Physics and Chemistry of Inorganic*

Clathrates, Chap.10, Ed. G. S. Nolas, Springer, 2014, p. 277 – 326.

[29] H. Mutka, M. M. Koza, M. R. Johnson, Z. Hiroi, J.-I. Yamaura and Y. Nagao, *Phys. Rev. B* **78**, 104307 (2008).

[30] M. M. Koza, A. Leithe-Jasper, E. Sischka, W. Schnelle, H. Borrmann, H. Mutka and Yu. Grin, *Phys. Chem. Chem. Phys.* **16**, 27119 (2014).

[31] Y. Bouyrie, C. Candolfi, S. Pailhès, M. M. Koza, B. Malaman, A. Dauscher, J. Tobola, O. Boisron, L. Saviot and B. Lenoir, *Phys. Chem. Chem. Phys.* **17**, 19751 (2015).

[32] U. Aydemir, C. Candolfi, A. Ormeci, Y. Oztan, M. Baitinger, N. Oeschler, F. Steglich and Yu. Grin, *Phys. Rev. B* **84**, 195137 (2011).

[33] M. A. Avila, K. Suekuni, K. Umeo, H. Fukuoka, S. Yamanaka and T. Takabatake, *Appl. Phys. Lett.* **92**, 041901 (2008).

[34] M. A. Avila, K. Suekuni, K. Umeo, H. Fukuoka, S. Yamanaka and T. Takabatake, *Phys. Rev. B* **74**, 125109 (2006).

Figure Captions

Figure 1: (a) Crystal structure of $BaGe_5$: (a) view along [100] displaying channels and covalently-bonded Ge layers; (b) view along [010]. The Ba1 atoms (black) are inside night blue dodecahedra, Ba2 atoms (green) are in the channels and Ba3 atoms (yellow) are in open Ge_{24} polyhedra. Alternatively occupied Ge sites with two connection patterns are represented in red color and transparent one.

Figure 2: Atomic displacement ellipsoids of $BaGe_5$ based on the structure model tabulated in Table I. Ba1, Ba2 and Ba3 atoms are shown in black, green and yellow colors, respectively, while Ge4 and Ge5 atoms are shown as red and the other Ge atoms as grey.

Figure 3: Elastic structure factor calculated from energy-resolved data and simulated neutron diffraction pattern of $BaGe_5$. The simulated pattern has been obtained by assuming a constant wavelength of λ = 4.14 Å and by using arbitrary half-width parameters to account for the resolution of the instrument. The asterisk marks the additional reflection due to elemental Ge observed slightly below 80° in agreement with PXRD data.

Figure 4: Magnification of the low-energy region of the $S(Q,\omega)$ map of $BaGe_5$ measured at 300 K. The arrows show the position of the three main maxima observed below ~15 meV.

Figure 5: (a) Generalized density of states $G(\omega)$ for $BaGe_5$ as derived from IN6 measurements at 300 (●) and 100 K (■). Both spectra have been normalized to equal intensity. The lack of data near 22.5 meV (marked by a black arrow) is due to the second-order elastic scattering coming from the monochromator of the IN6@ILL setup becoming detectable at low

temperatures. The data collected at 100 K have been cut at ~32 meV due to the poor statistics above this energy. (b) Debye plot ($G(\omega)/(\hbar\omega)^2$ vs. $\hbar\omega$) that stresses the low-energy peaks likely associated with Ba-weighted modes. Note that, in both panels, the data were normalized to suppress the effect of the Debye-Waller factors *i.e.* of the thermal displacement parameters of the atoms.

Figure 6: Energy of the main peaks for $BaGe_5$ measured at 300 (●) and 100 K (■). The hardening of the peak position upon cooling is compared to the prediction of the quasiharmonic model represented by the solid black lines.

Figure 7: Plot of C_p/T^3 as a function of T for $BaGe_5$ to highlight the additional contribution superimposed on the Debye background. The red dotted line stands for the experimental data while the solid black line is the best fit to the data according to Eq.(2).

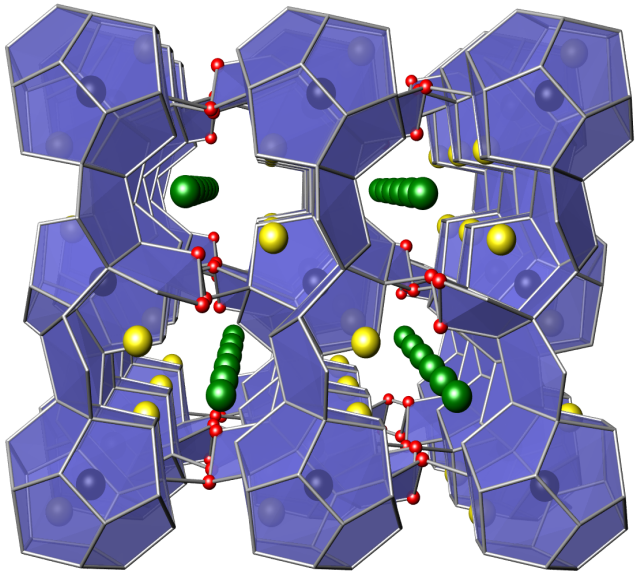

(a)

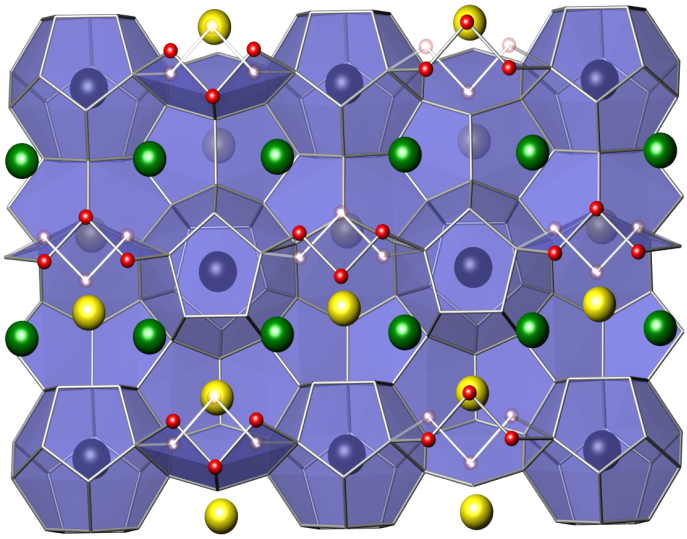

(b)

Figure 1

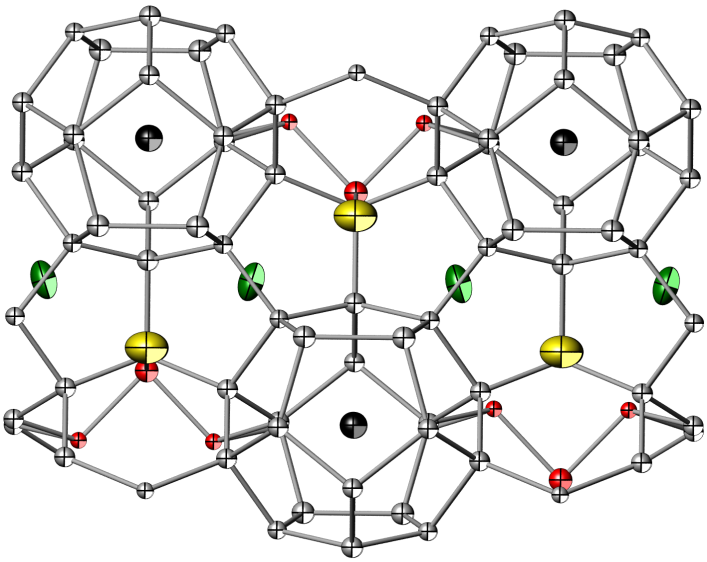

Figure 2

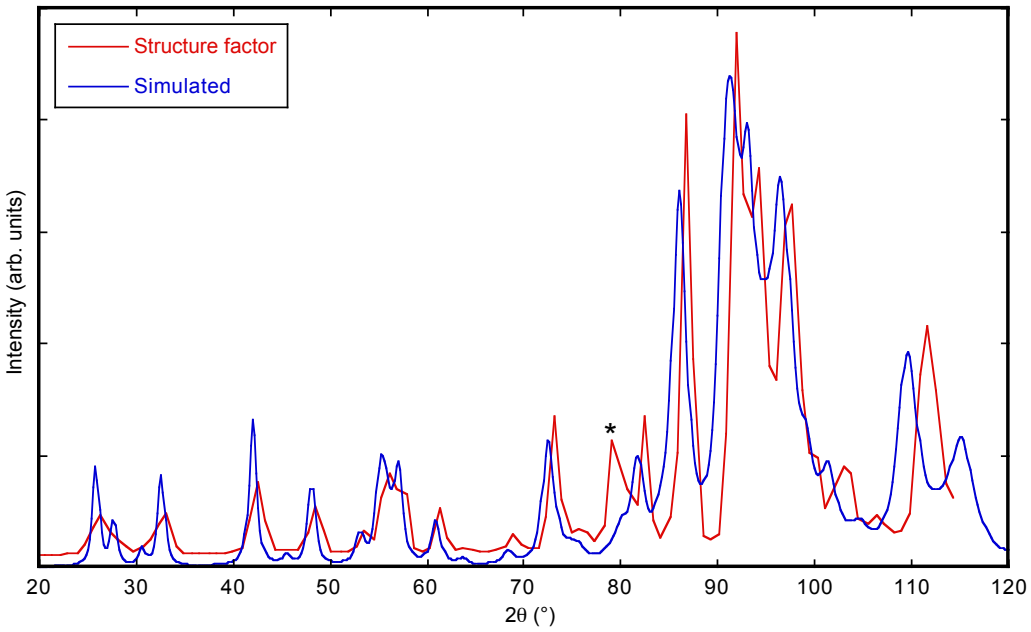
Structure factor
Simulated
Intensity (arb. units)
2θ (°)
20
30
40
50
60
70
80
90
100
110
120
*

Figure 3

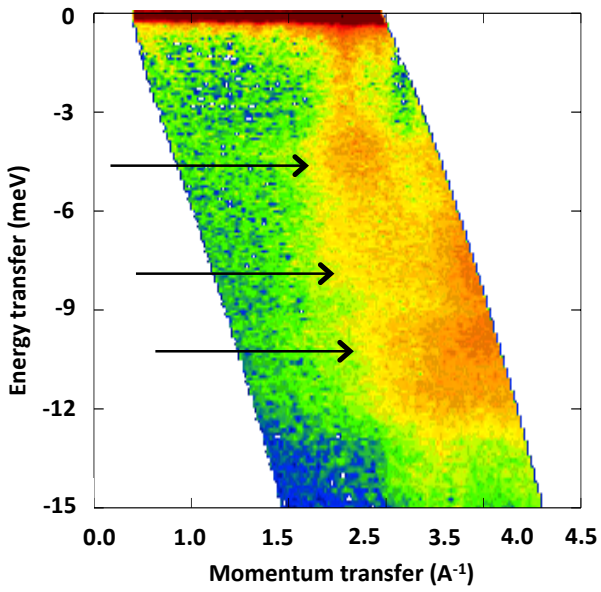
0
-3
-6
-9
-12
-15
Energy transfer (meV)
0.0
1.0
1.5
2.5
3.5
4.0
4.5
Momentum transfer (A-1)

Figure 4

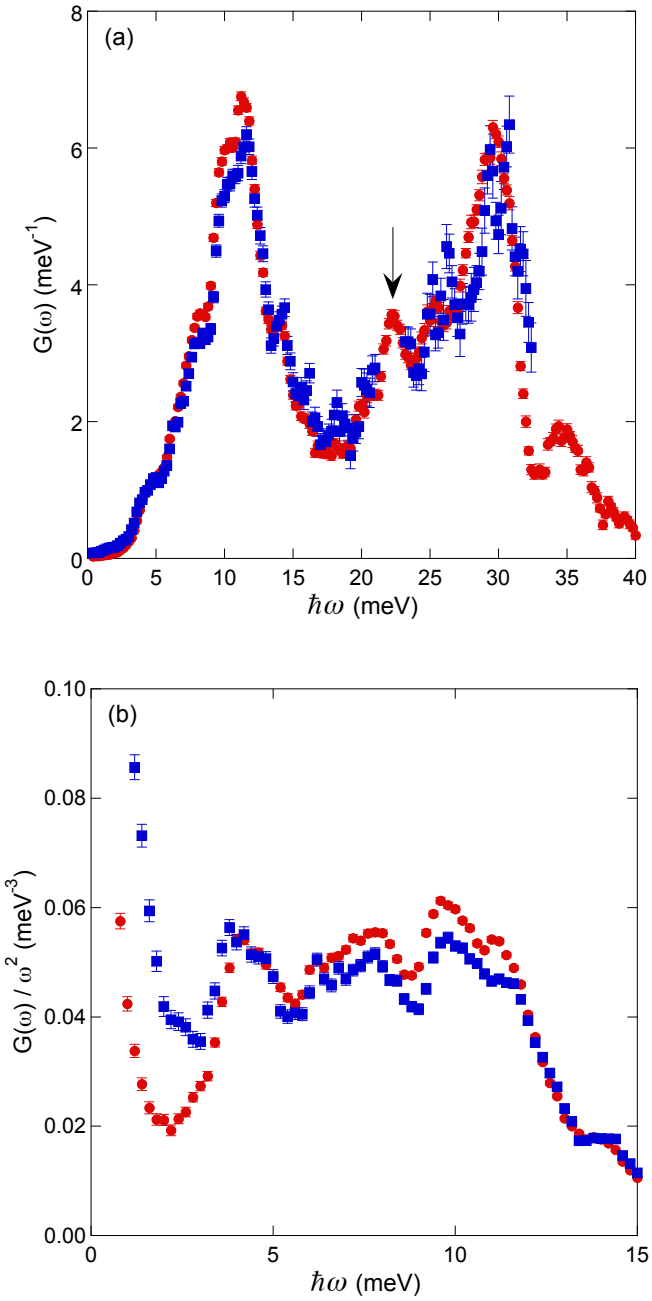

Figure 5

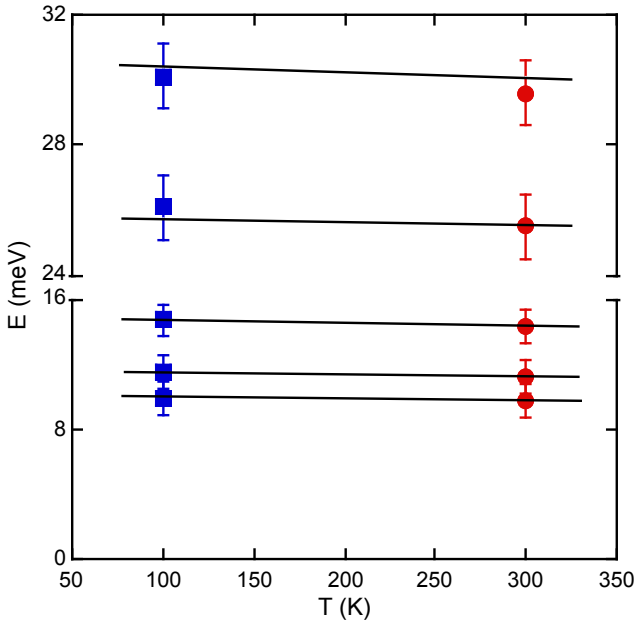

Figure 6

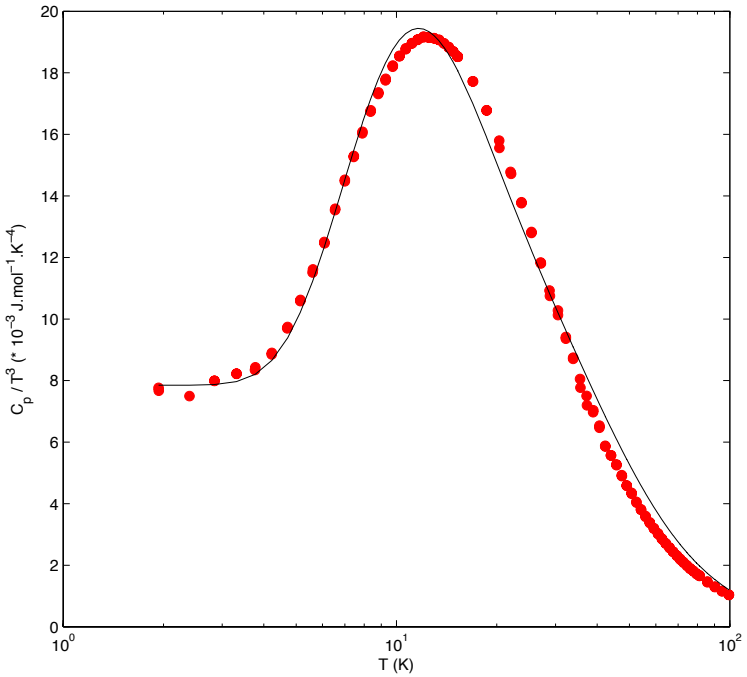

Figure 7